**Electronic supporting information**

# $NiN_3$-Embedded $MoS_2$ Monolayer as a Promising Electrocatalyst with High Activity for Oxygen Evolution Reaction: A Computational Study

*Xinyi Li,[a] Dongxu Jiao,[a] Yanyu Liang,[b,*] Jingxiang Zhao[a,*]*

*[a] College of Chemistry and Chemical Engineering, and Key Laboratory of Photonic and Electronic Bandgap Materials, Ministry of Education, Harbin Normal University, Harbin, 150025, P. R. China*

*[b] Jiangsu key Laboratory of Electrochemical Energy Storage Technologies, College of Material Science and Technology Nanjing University of Aeronautics and Astronautics Nanjing 210016, P. R. China*

*[*] To whom correspondence should be addressed. Email: liangyy403@126.com (YL) and xjz_hmily@163.com or zhaojingxiang@hrbnu.edu.cn (JZ)*

**Computional Details on Dissolution Potential and Overpotential**

To evaluate the stability of $NiN_3$@$MoS_2$ monolayer in realistic reaction conditions, such as strong acidic media and working potential, we computed the dissolution potentials ($U_{dis}$, in V) of Ni in $N_3$@$MoS_2$ monolayer at pH=0, which was defined as: $U_{dis} = U_{Ni}^{0} + \left[E_{Ni,bulk} - \left(E_{NiN_3@MoS_2} - E_{N_3@MoS_2}\right)\right]/ne$, where $U_{Ni}^{0}$ is the standard dissolution potential of Ni in the bulk form (–0.26 V), $N_3@MoS_2$ is the doped $MoS_2$ monolayer by substituting three S atoms with three N dopants, and *n* is the coefficient for the aqueous dissolution reaction: $Ni + 2H^+ \leftrightarrow Ni^{2+} + H_2$, namely, *n* equals to 2. According to this definition, the $U_{dis}$ value of Ni in $NiN_3$@$MoS_2$ monolayer is computed to be about 0.30 V.

On the other hand, the overpotential (η) value of OER was obtained according to the following equation: $\eta = U_L - U_0$, where $U_0$ is the computed equilibrium potential of OER ($U_0$ = 1.23 V), and $U_L$ is the limiting potential of OER on $NiN_3$@$MoS_2$ monolayer ($U_L = \Delta G_{max}/e$, V). Since the $\Delta G_{max}$ value for OER on $NiN_3$@$MoS_2$ monolayer was computed to be 1.68 eV, the computed $U_L$ is [(1.68 eV)/*e* – 1.23 V) = 0.45 V]. Thus, the negative overpotential (−η) of OER on $NiN_3$@$MoS_2$ monolayer is −0.45 V, which is much smaller than the $U_{dis}$ value of Ni (0.30 V), suggesting that Ni within the $NiN_3$@$MoS_2$ framework can survive under the realistic experimental conditions of OER, and thus ensuring their excellent long-term stability.

**Table S1.** The computed binding energies ($E_{bind}$, eV), shortest distances between TM and N atoms ($d_{TM-N}$, Å), charge transfer ($Q$, |e|) from TM to substrate, height ($h$, Å) of TM outward from $MoS_2$ monolayer, and overpotential (η, V) for various $TMN_x$ ($x$ = 1-3) moieties embedded into $MoS_2$ monolayer.

| | $E_{bind}$ | $d_{TM-N}$ | $Q$ | $h$ | η |
|---|---|---|---|---|---|
| $MnN_3$ | –5.68 | 1.91 | 1.18 | 0.42 | 1.59 |
| $FeN_3$ | –6.17 | 1.92 | 1.17 | 0.42 | 0.87 |
| $CoN_3$ | –5.63 | 1.89 | 0.98 | 0.35 | 0.63 |
| $NiN_3$ | –5.35 | 1.92 | 0.81 | 0.31 | 0.45 |
| $CuN_3$ | –3.38 | 1.98 | 0.78 | 0.45 | 0.85 |
| $RhN_3$ | –5.29 | 2.00 | 0.38 | 0.40 | 1.12 |
| $PdN_3$ | –3.14 | 2.17 | 0.58 | 0.75 | 0.65 |
| $PtN_3$ | –4.19 | 2.05 | 0.61 | 0.89 | 1.40 |
| $MnN_2$ | –4.87 | 1.95 | 1.10 | 0.97 | 1.50 |
| $FeN_2$ | –4.06 | 1.85 | 0.96 | 0.75 | 1.45 |
| $CoN_2$ | –4.99 | 1.89 | 0.77 | 0.81 | 1.26 |
| $NiN_2$ | –4.93 | 1.86 | 0.64 | 0.73 | 0.59 |
| $CuN_2$ | –3.31 | 1.94 | 0.71 | 0.90 | 0.89 |
| $RhN_2$ | –5.13 | 2.04 | 0.53 | 1.45 | 0.94 |
| $PdN_2$ | –3.07 | 2.15 | 0.42 | 1.45 | 0.67 |
| $PtN_2$ | –4.13 | 2.11 | 0.35 | 1.46 | 0.91 |
| $MnN_1$ | –3.27 | 1.90 | 0.99 | 0.95 | 1.28 |
| $FeN_1$ | -3.97 | 1.85 | 0.82 | 0.78 | 0.99 |
| $CoN_1$ | -4.19 | 1.82 | 0.68 | 0.79 | 0.98 |
| $NiN_1$ | –4.57 | 1.81 | 0.57 | 0.72 | 0.72 |
| $CuN_1$ | –3.13 | 1.89 | 0.61 | 1.06 | 0.82 |
| $RhN_1$ | –4.56 | 1.90 | 0.41 | 1.05 | 0.89 |
| $PdN_1$ | –2.92 | 2.02 | 0.39 | 1.41 | 0.84 |
| $PtN_1$ | –3.85 | 1.93 | 0.26 | 1.60 | 1.14 |

**Table S2.** The comparison of overpotential for various reported metal-doped $MoS_2$ materials.

| catalysts | overpotential |
|---|---|
| Co-doped $MoS_2$ | 0.22 V[1] |
| $Pd_2$@$MoS_2$ | 0.32 V[2] |
| $NiN_3$@$MoS_2$ in this work | 0.45 V |
| Pt@T1-vacancy | 0.46 V[3] |
| Co-Ni-P@$MoS_2$ | 0.68 V[4] |
| Ni-doped $MoS_2$ | 1.08 V[5] |
| Fe-doped $MoS_2$ | 1.57 V[6] |

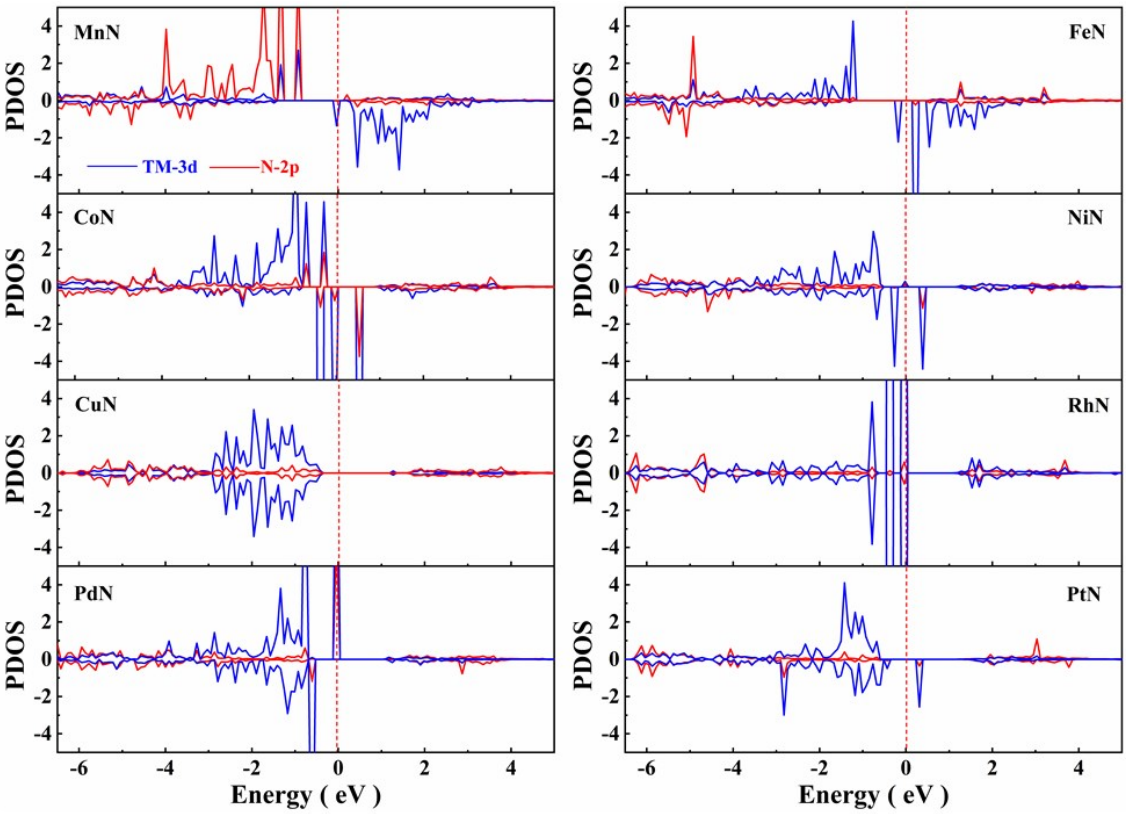
MnN
FeN
CoN
NiN
CuN
RhN
PdN
PtN
TM-3d
N-2p
PDOS
Energy ( eV )

(a)

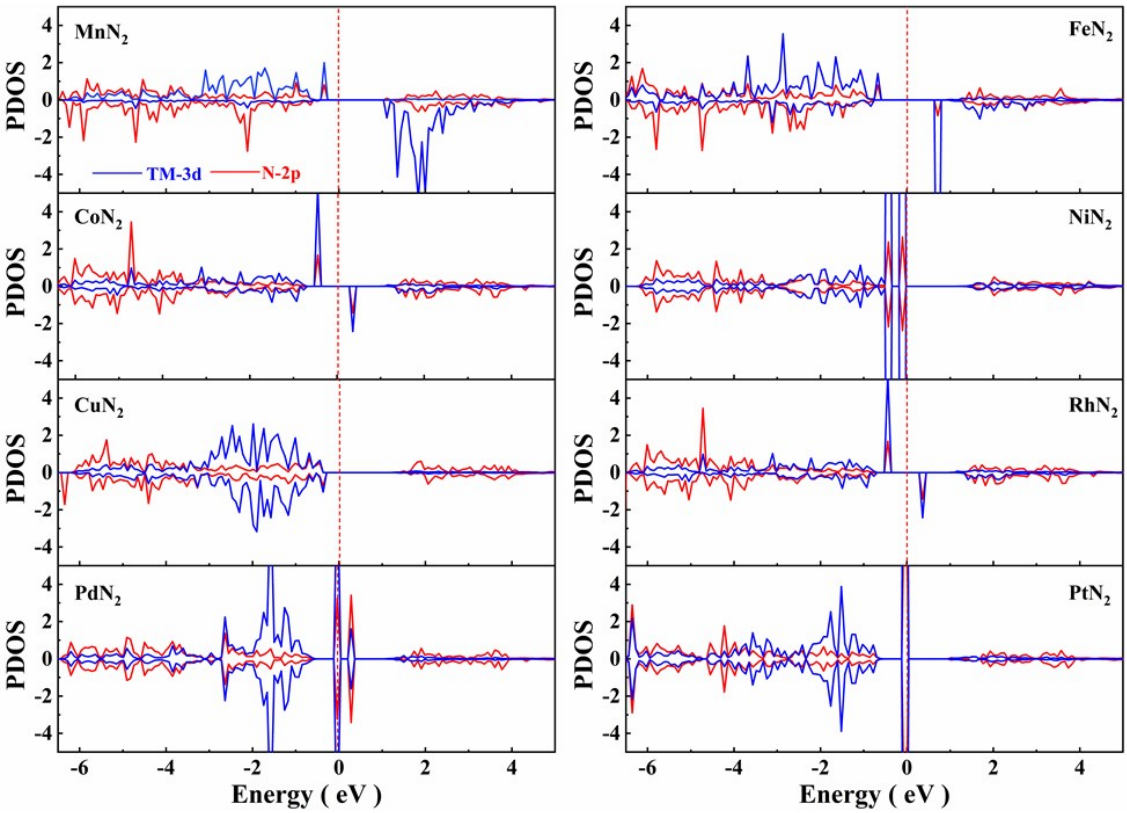
MnN2
FeN2
CoN2
NiN2
CuN2
RhN2
PdN2
PtN2
TM-3d
N-2p
PDOS
Energy ( eV )

(b)

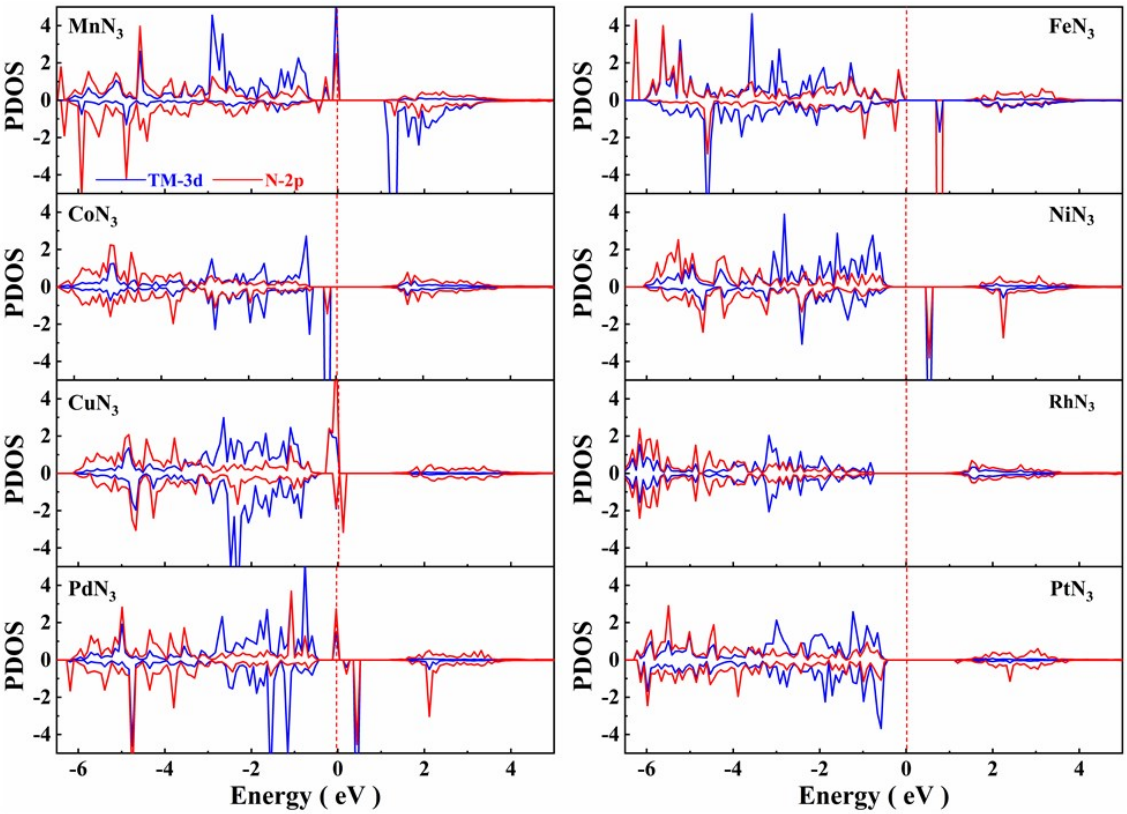


(c)

**Fig. S1**. The computed projected density of states (PDOSs) of (a) $TMN_1$, (b) $TMN_2$, and (c) $TMN_3$ moieties embedded into $MoS_2$ monolayer. The Fermi level was set to zero in red dotted line.

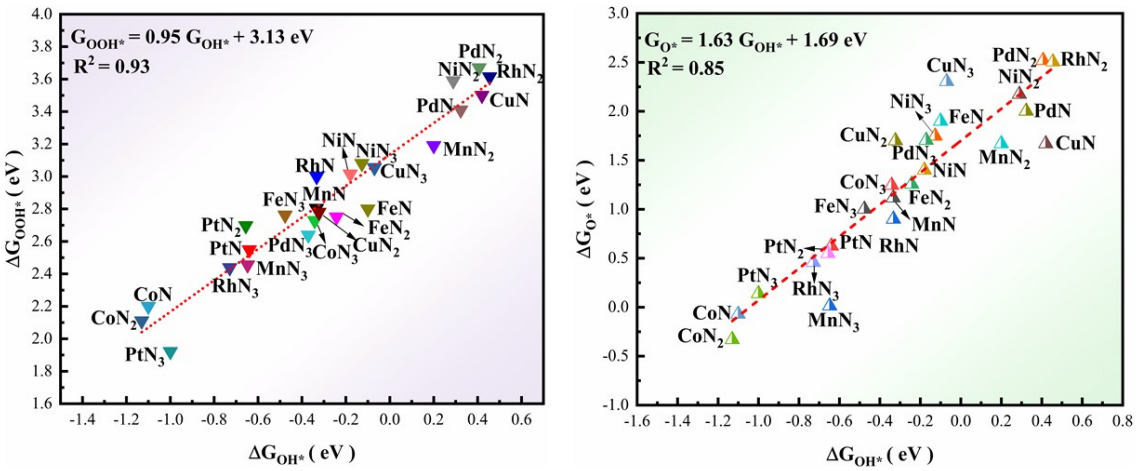


(a) (b)

**Fig. S2**. The scaling relationships for Gibbs adsorption free energy of (a) $OOH^*$ *vs* $OH^*$ and (b) $O^*$ *vs* $OH^*$ species on $TMN_x$@$MoS_2$ ($x$ = 1-3) materials.

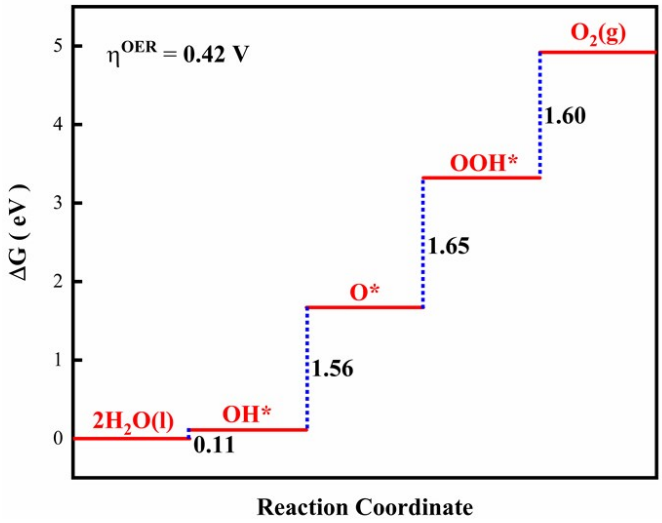


**Fig. S3**. The computed free energy profile for OER on $NiN_3$@$MoS_2$ catalyst with solvent effect.

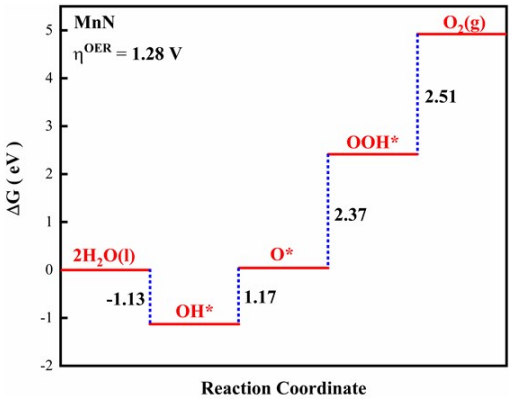
MnN
$\eta^{OER}$ = 1.28 V
$2H_2O(l)$
-1.13
OH*
1.17
O*
2.37
OOH*
2.51
$O_2(g)$
ΔG ( eV )
Reaction Coordinate

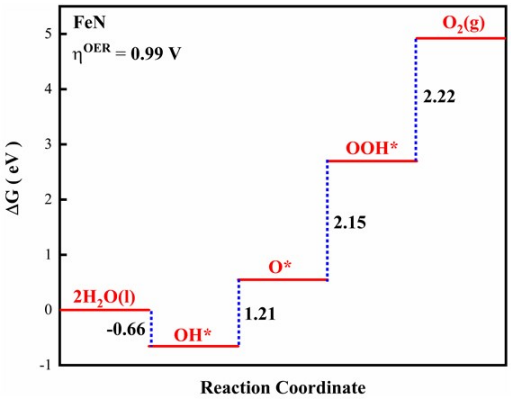
FeN
$\eta^{OER}$ = 0.99 V
$2H_2O(l)$
-0.66
OH*
1.21
O*
2.15
OOH*
2.22
$O_2(g)$
ΔG ( eV )
Reaction Coordinate

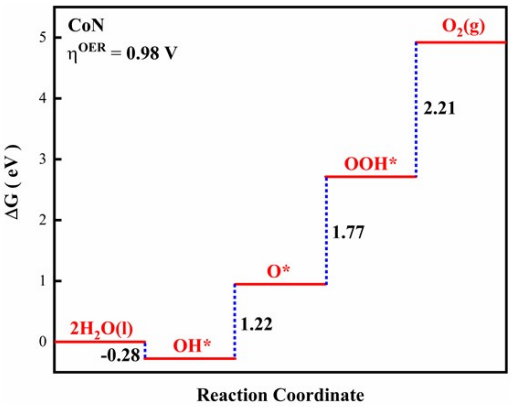
CoN
$\eta^{OER}$ = 0.98 V
$2H_2O(l)$
-0.28
OH*
1.22
O*
1.77
OOH*
2.21
$O_2(g)$
ΔG ( eV )
Reaction Coordinate

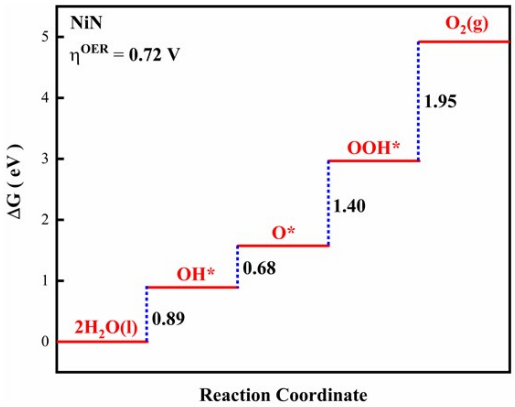
NiN
$\eta^{OER}$ = 0.72 V
$2H_2O(l)$
0.89
OH*
0.68
O*
1.40
OOH*
1.95
$O_2(g)$
ΔG ( eV )
Reaction Coordinate

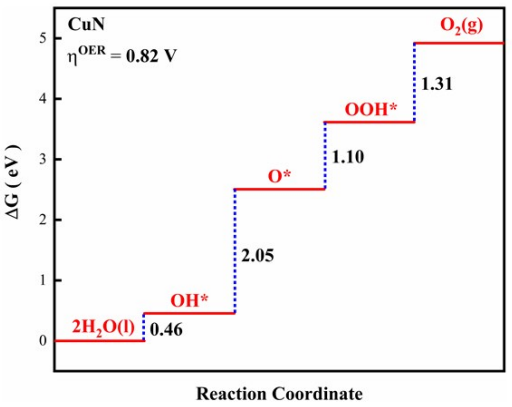
CuN
$\eta^{OER}$ = 0.82 V
$2H_2O(l)$
0.46
OH*
2.05
O*
1.10
OOH*
1.31
$O_2(g)$
ΔG ( eV )
Reaction Coordinate

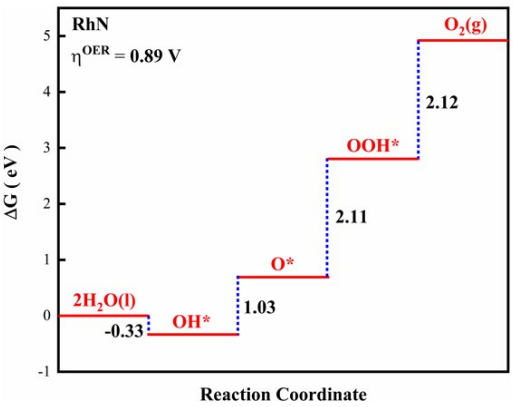
RhN
$\eta^{OER}$ = 0.89 V
$2H_2O(l)$
-0.33
OH*
1.03
O*
2.11
OOH*
2.12
$O_2(g)$
ΔG ( eV )
Reaction Coordinate

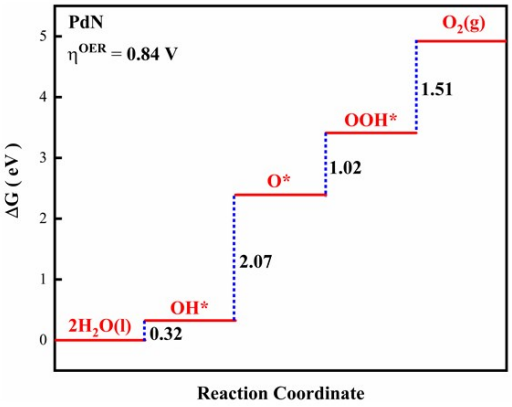
PdN
$\eta^{OER}$ = 0.84 V
$2H_2O(l)$
0.32
OH*
2.07
O*
1.02
OOH*
1.51
$O_2(g)$
ΔG ( eV )
Reaction Coordinate

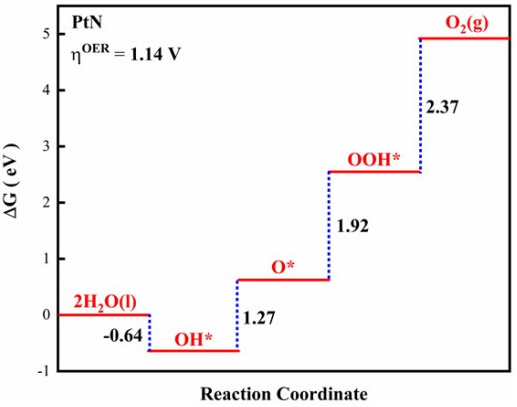
PtN
$\eta^{OER}$ = 1.14 V
$2H_2O(l)$
-0.64
OH*
1.27
O*
1.92
OOH*
2.37
$O_2(g)$
ΔG ( eV )
Reaction Coordinate

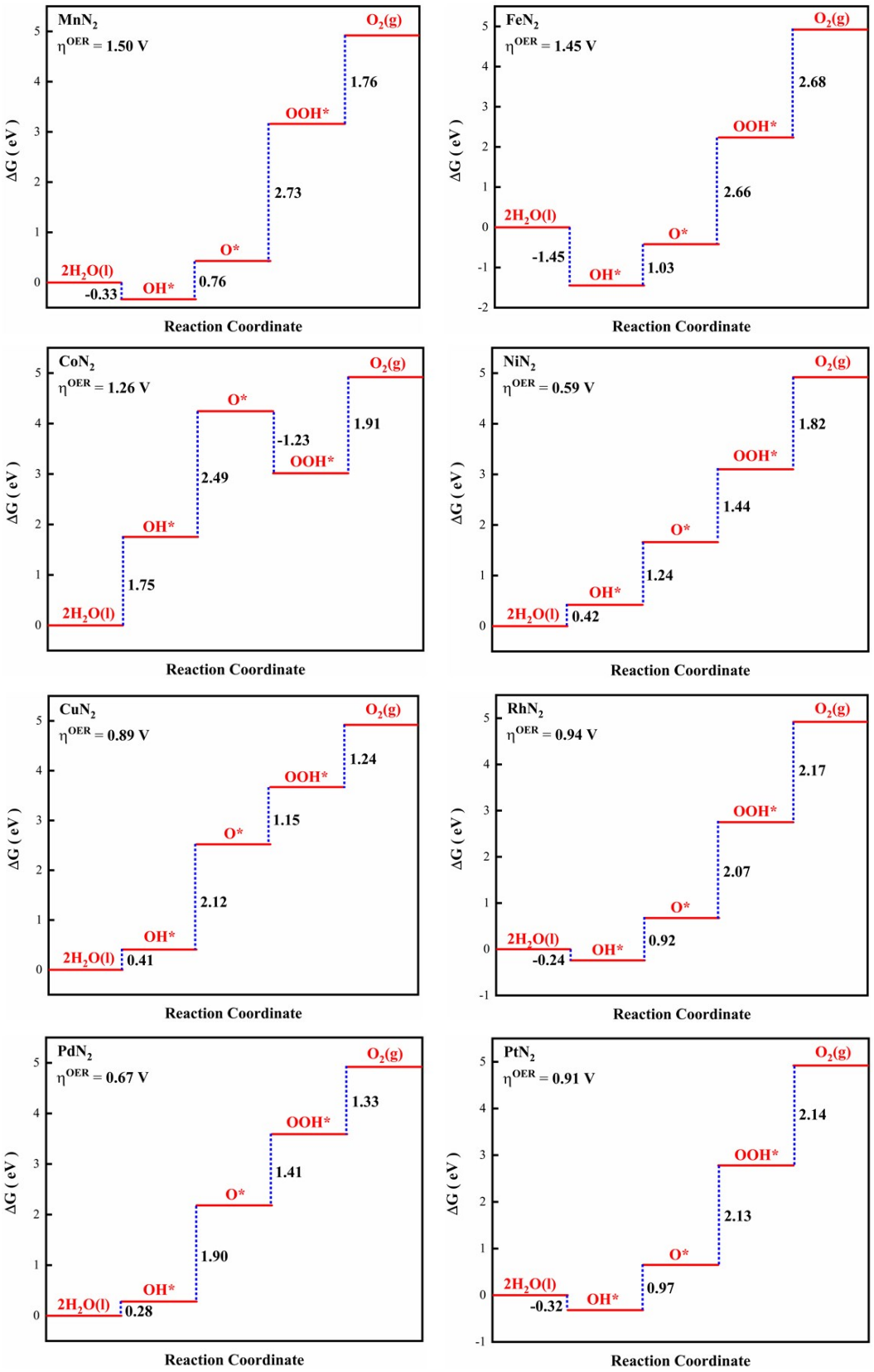


**Fig. S4.** The computed free energy profiles for OER on $TMN_1$ and $TMN_2$ moieties embedded into $MoS_2$ monolayer.

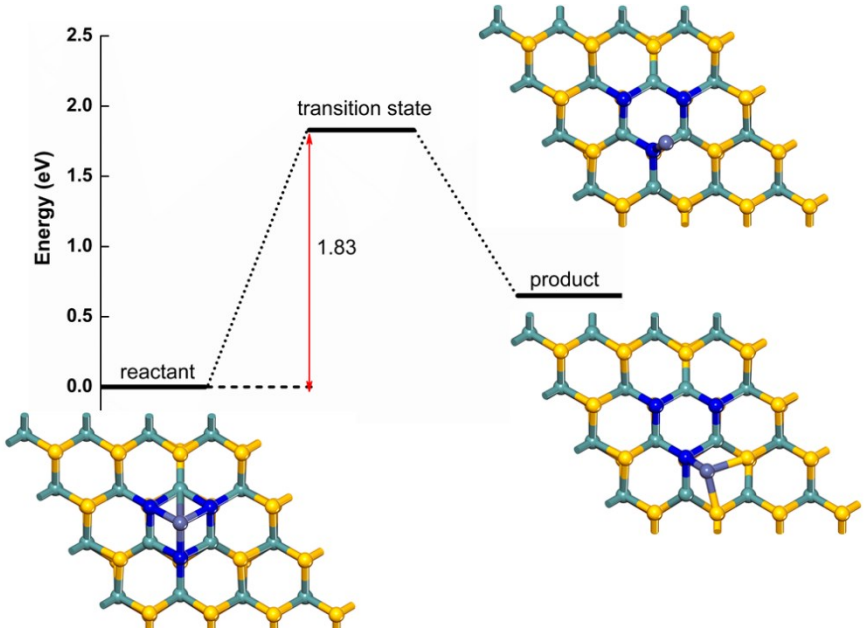


**Fig. S5.** The computed reaction pathway for the diffusion of single Ni atom on $NiN_3$@$MoS_2$, and the atomic configurations of the involved reactant, transiton state, and product.

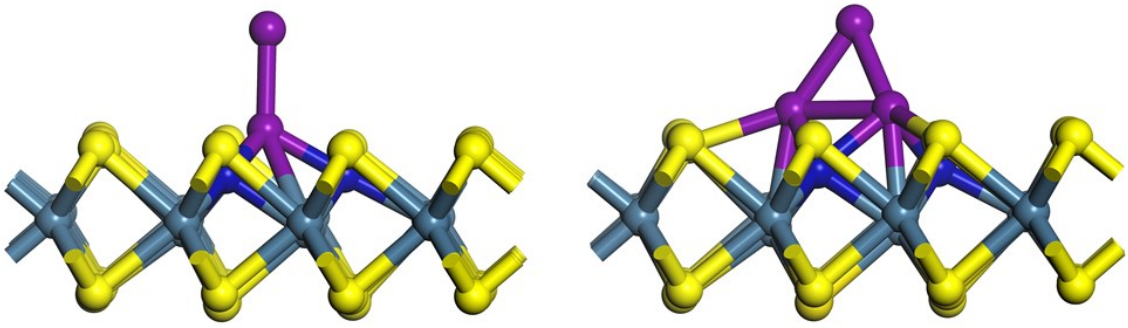

(a) $E_{bind}$ = –4.07 eV (b) $E_{bind}$ = –5.03 eV

**Fig. S6.** The optimized structures and the corresponding binding energies for (a) $Ni_2$ and (c) $Ni_3$ clusters anchored on doped $MoS_2$ monolayer with three N atoms. Cyan, yellow, purple, and blue balls represent Mo, S, TM, and N atoms, respectively.

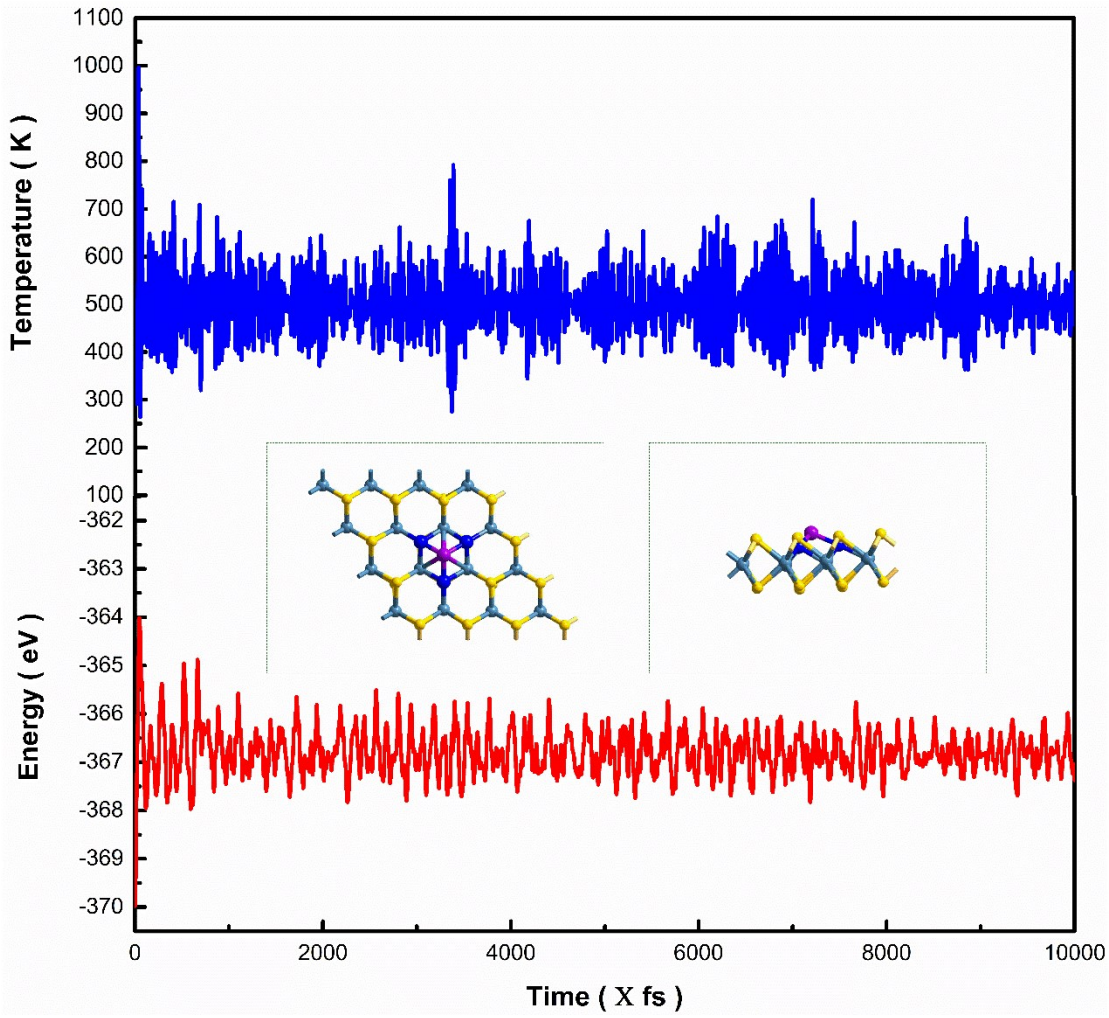


**Fig. S7.** The variations of temperature and energy versus the time for AIMD simulations of $NiN_3$@$MoS_2$, which is run under 500 K for 10 ps with a time step of 1 fs. Schematic diagrams of the atomic configurations after dynamics simulation (top and side views) are also given.

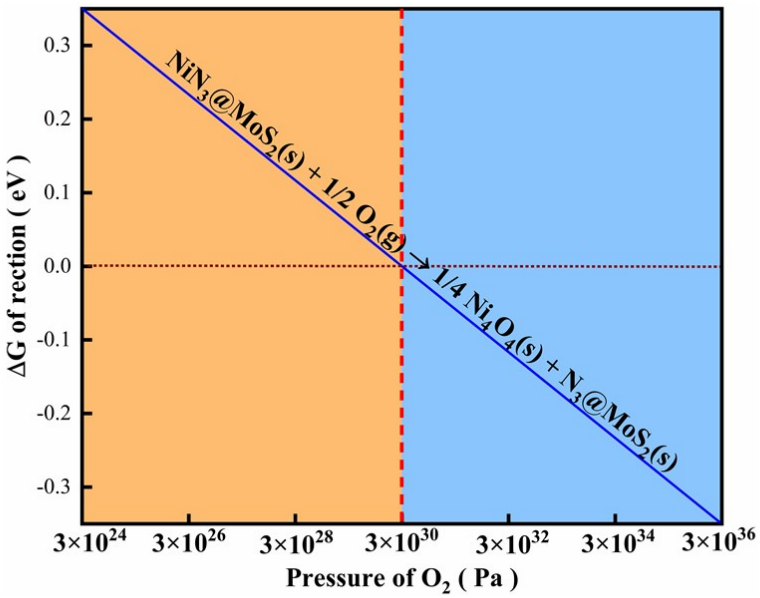


**Fig. S8.** Reaction Gibbs free energy of $NiN_3@MoS_2$ (*s*) + 1/2 $O_2$ (*g*) → $N_3@MoS_2$ (*s*) + 1/4 $Ni_4O_4$ (*s*) on $NiN_3/MoS_2$ surface versus $O_2$ pressure under 298 K, light yellow and light blue regions represent the formation of Ni SAC and $Ni_4O_4$ oxide, respectively.

The formation of Ni oxide on $NiN_3@MoS_2$ monolayer can be written by: $NiN_3@MoS_2$ (*s*) + 1/2 $O_2$ (*g*) → $N_3@MoS_2$ (*s*) + 1/4 $Ni_4O_4$ (*s*), in which the pressures of the solid states $NiN_3@MoS_2$, $N_3@MoS_2$, and $Ni_4O_4$ were set as zero. Thus, the partial $O_2$ pressure for the formation of Ni oxide on $NiN_3@MoS_2$ monolayer can be determined as follows:[3,4] $(P_{O_2})^{\frac{1}{2}} = e^{-\frac{\Delta G}{k_B T}}$, where $\Delta G$ is the free energy change for the formation of Ni oxide , $k_B$ is the Boltzmann constant, and T is the reaction temperature.

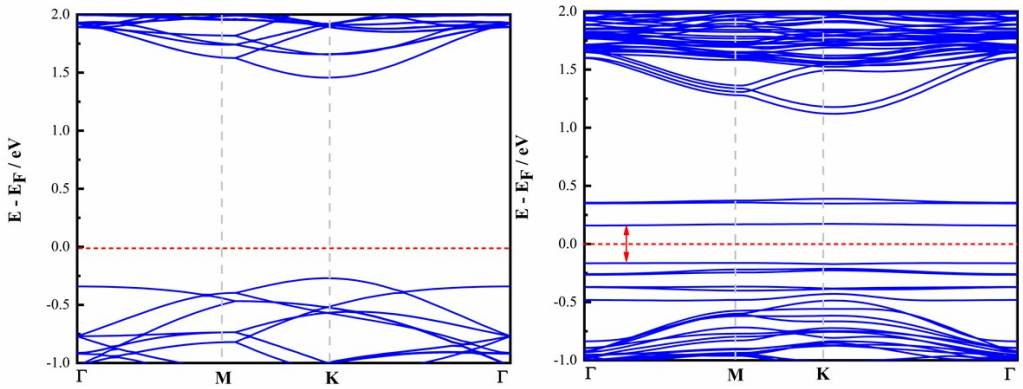


**Fig. S9**. The computed band structures of (a) pristine $MoS_2$ monolayer and (b) $NiN_3$@$MoS_2$ monolayer. The Fermi level was set to zero in dotted red line.

1 Q. Xiong, Y. Wang, P. F. Liu, L. R. Zheng, G. Wang, H. G. Yang, P. K. Wong, H. Zhang and H. Zhao, *Adv. Mater.*, 2018, 30, 1801450.

2. F. He, Y. Liu, Q. Cai and J. Zhao, *New J. Chem.*, 2020, **44**, 16135-16143.

3. X. Xu, H. Xu and D. Cheng, *Nanoscale*, 2019, 11, 20228–20237.

4. J. Bao, Y. Zhou, Y. Zhang, X. Sheng, Y.Wang, S. Liang, C. Guo, W. Yang, T. Zhuang and Y. Hu, *J. Mater. Chem. A*, 2020, **8**, 22181-22190.

5. Y. Wang, W. Sun, X. Ling, X. Shi, L. Li, Y. Deng, C. An and X. Han, *Chem. – A Eur. J.*, 2020, 26, 4097-4103.

6. B. Tang, Z. G. Yu, H. L. Seng, N. Zhang, X. Liu, Y.-W. Zhang, W. Yang and H. Gong, *Nanoscale*, 2018, 10, 20113-20119.